RESEARCH PAPER

Silver Cholate–Based Metallogel with High Structural Integrity, Biocompatibility, and Antimicrobial Activity for Skin-Relevant Applications

Kamalasivam S[1], Nandhakumar S[2*]

[1]Faculty of Pharmacy, Dr. M.G.R. Educational and Research Institute, Velappanchavadi, Chennai-600077, Tamil Nadu, India

[2*]Faculty of Pharmacy, Dr. M.G.R. Educational and Research Institute, Velappanchavadi, Chennai-600077, Tamil Nadu, India

Corresponding Author: Nandhakumar S. Mail ID: nandhakumar.pharm@drmgrdu.ac.in

ABSTRACT

Metallogels derived from low-molecular-weight gelators have emerged as versatile soft materials owing to their self-assembled architectures and stimuli-responsive behavior. Among them, bile salt–based metallogels offer unique advantages due to their intrinsic amphiphilicity, biocompatibility, and availability from renewable sources. In the present study, we report the facile preparation and comprehensive characterization of a silver cholate–based metallogel formed through coordination-driven self-assembly between silver ions and sodium cholate in aqueous media. Metallogel formation was achieved without multistep synthesis or external cross-linkers, highlighting a simple and scalable approach. Systematic variation of silver ion concentration resulted in distinct gel states with tunable opacity and structural robustness.

Fourier-transform infrared (FTIR) spectroscopy confirmed coordination between Ag^+ ions and the carboxylate groups of cholate, as evidenced by characteristic shifts in asymmetric and symmetric stretching frequencies, while UV–Visible spectroscopy supported silver incorporation within the supramolecular framework through broad visible-region absorption features. Scanning electron microscopy (SEM) revealed a densely interconnected nanostructured network, and rheological analysis quantitatively confirmed gel-like viscoelastic behavior, providing insight into the self-supporting nature and mechanical stability of the metallogel. Cytotoxicity evaluation using the HaCaT human keratinocyte cell line demonstrated a clear concentration-dependent safety profile, with selected formulations exhibiting excellent biocompatibility up to 1% concentration. Furthermore, the silver metallogel displayed pronounced antibacterial activity against *Cutibacterium acnes* and antifungal efficacy against *Malassezia furfur*, supported by rapid log-reduction and low minimum inhibitory concentration (MIC) values.

Overall, the combination of coordination-driven assembly, nanostructured morphology, biological compatibility, and antimicrobial potency positions this silver cholate metallogel as a promising soft material for topical and skin-related biomedical applications.

Keywords: Silver metallogel; Sodium cholate; Metallogel self-assembly; FTIR spectroscopy; Cytotoxicity; Antibacterial activity; Antifungal activity.

How to cite this article: Kamalasivam S, Nandhakumar S. Silver Cholate–Based Metallogel with High Structural Integrity, Biocompatibility, and Antimicrobial Activity for Skin-Relevant Applications. Int J Drug Deliv Technol. 2026;16(14s): 28-40. DOI: 10.25258/ijddt.16.14s.5

Introduction

The past two decades have witnessed remarkable progress in supramolecular hydrogels, particularly those assembled from low-molecular-weight gelators (LMWGs), owing to their reversible non-covalent interactions, structural tunability, and stimuli-responsive behavior. Metallohydrogels, in which metal ions serve as both structural nodes and functional elements, constitute a particularly versatile subclass, enabling applications in catalysis, sensing, drug delivery, and tissue engineering [1–7].

Bile salts, such as sodium cholate, represent an underexplored yet highly promising family of LMWGs [8-10]. Derived from cholesterol metabolism, these molecules exhibit a rigid steroidal backbone with pronounced facial amphiphilicity: a hydrophilic α-face bearing three hydroxyl groups and a hydrophobic β-face populated by methyl substituents. This unique topology enables bile salts to form micelles, vesicles, and in the presence of appropriate metal ions extended supramolecular networks in aqueous environments [11-13]. Unlike many synthetic gelators requiring complex

multi-step synthesis, sodium cholate is commercially available, biodegradable, cost-effective, and inherently biocompatible, making it an attractive scaffold for sustainable biomaterials.

Silver ions (Ag^+) are particularly appealing as coordinating metals due to their well-established broad-spectrum antimicrobial activity, which arises from multiple mechanisms including disruption of bacterial cell membranes, inhibition of respiratory enzymes, and generation of reactive oxygen species (ROS) [14–20]. Silver-based materials have long been employed in wound care (e.g., silver sulfadiazine creams) and medical device coatings; however, uncontrolled release often leads to local cytotoxicity, delayed healing, and argyria [21-25]. Incorporating Ag^+ within a supramolecular hydrogel matrix offers a promising strategy to achieve sustained, localized delivery while minimizing systemic toxicity [15,16].

Despite these advantages, systematic studies of silver cholate metallohydrogels remain limited compared to gels formed with divalent metals (e.g., Zn^{2+}, Cu^{2+}). Existing reports on bile salt metallogels have primarily focused on nanoparticle templating [17-19], dye adsorption or energy transfer, with comparatively little attention devoted to detailed structural characterization, concentration-dependent biocompatibility, and targeted antimicrobialperformance against skin-relevant pathogens such as *Cutibacterium acnes* (acne-associated) and *Malassezia furfur* (dandruff/seborrheic dermatitis-associated) [26-35]

The present study addresses these gaps by reporting the facile, one-pot preparation of silver cholate metallohydrogels and their comprehensive physicochemical and biological evaluation. We demonstrate that coordination between Ag^+ and the cholate carboxylate group drives self-assembly into a nanostructured network, as confirmed by FTIR spectroscopy and scanning electron microscopy (SEM). Cytotoxicity profiling on HaCaT human keratinocytes establishes a clear therapeutic window, while antimicrobial assays reveal rapid and potent activity against key skin pathogens. Collectively, these results position silver cholate metallohydrogels as promising candidates for next-generation topical antimicrobial formulations. Unlike many reported silver-based soft materials, the present system integrates coordination-driven gelation, concentration-resolved cytotoxicity profiling, and skin-pathogen–specific antimicrobial evaluation within a single bile salt–based metallogel platform

2. Materials and Methods

2.1 Materials

Sodium cholate (≥99% purity) and silver salts were used as received without further purification. Deionized water was employed for all solution preparations. Dulbecco's Modified Eagle Medium (DMEM), fetal bovine serum (FBS), trypsin–EDTA solution, phosphate-buffered saline (PBS), and MTT reagent were used for cytotoxicity studies. All cell culture reagents were of cell-culture grade. Microbiological media and reference antimicrobial agents used for antibacterial and antifungal studies were obtained from standard commercial suppliers.

2.2 Preparation of Silver Cholate Metallogel

Silver cholate metallogels were prepared through a simple aqueous mixing protocol. Sodium cholate was dissolved in deionized water to obtain a clear stock solution under gentle stirring at room temperature. A separate aqueous solution of the silver salt was prepared freshly prior to use. The silver salt solution was added slowly to the sodium cholate solution under ambient conditions with gentle mixing.

Gelation occurred spontaneously within minutes, depending on the molar ratio of sodium cholate to Ag^+ ions. A series of formulations with varying metal-to-ligand ratios were prepared and coded as **SC-01 to SC-05**, corresponding to increasing silver ion content. The resulting systems ranged from clear sols to opaque, self-supporting metallogels. Gel formation was confirmed by the vial inversion test, wherein no flow was observed upon inversion of the container.

Visual appearance, opacity, and stability of the metallogels were documented photographically to assess concentration-dependent gel behavior. All samples were stored at room temperature and characterized without further aging unless otherwise stated.The preparation strategy and coordination-driven self-assembly process involved in silver cholate metallogel formation are schematically illustrated in **Figure 1**.The gelation parameters, minimum gelation concentration, opacity, and stability of formulations SC-01 to SC-05 are summarized in **Table 1.**

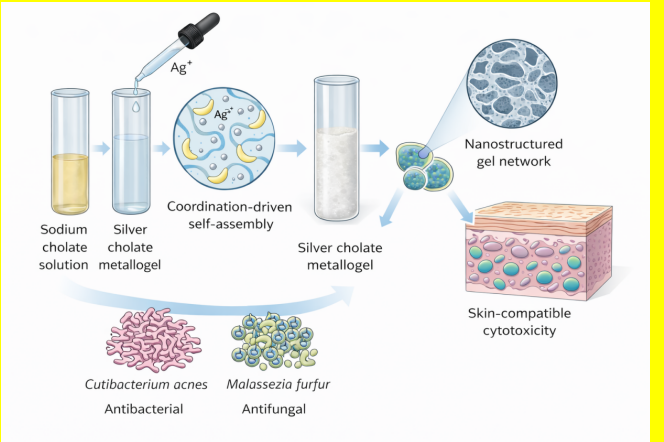

Figure 1. A schematic illustration showing the preparation of silver cholate metallogel via dropwise addition of Ag^+ ions into an aqueous sodium cholate solution, leading to coordination-driven self-assembly and formation of a nanostructured metallogel network. The graphical abstract highlights key features including Ag–carboxylate coordination, gel network formation, and dual antibacterial–antifungal activity with skin-compatible cytotoxicity.

Table 1. Gelation parameters for SC-01 to SC-05 formulations.

Formulation	Ag^+:Cholate (molar)	MGC (wt %)	Gelation Time (min)	Opacity (AU at 600 nm)	Stability (days at 25 °C)
SC-01	1:1	5.2	10	0.12	>30
SC-02	0.75:1	4.8	7	0.28	>30
SC-03	0.5:1	4.5	5	0.45	>30
SC-04	0.25:1	4.5	3	0.67	>30
SC-05	Excess Ag^+	4.6	2	0.92	>30

2.3 Fourier Transform Infrared (FTIR) Spectroscopy

FTIR spectroscopy was employed to investigate coordination interactions between silver ions and sodium cholate during metallogel formation. Spectra of sodium cholate, silver salt precursor, and dried silver cholate metallogel samples were recorded in transmittance mode (%T) over the range of 4000–400 cm^{-1}.

Samples were prepared by drying aliquots of the respective solutions or gels under ambient conditions. Spectral data were analyzed with particular emphasis on the carboxylate stretching region to evaluate changes in asymmetric (ν_as) and symmetric (ν_s) COO^- vibrations. Shifts in these bands and the appearance of low-frequency metal–oxygen vibrations were used to infer coordination modes between Ag^+ and cholate ligands.

2.4 Scanning Electron Microscopy (SEM)

The internal morphology of the silver cholate metallogel was examined using scanning electron microscopy. Gel samples were carefully dried to preserve the underlying network structure and mounted on conductive stubs. Prior to imaging, samples were sputter-coated with a thin conductive layer to minimize charging effects.

SEM images were acquired at an accelerating voltage of 15 kV. Micrographs were recorded at various magnifications to examine surface texture, particle distribution, and network connectivity. The observed nanostructured features were correlated with the macroscopic mechanical stability of the metallogel.

2.5 Cytotoxicity Evaluation Using HaCaT Cell Line

2.5.1 Cell Culture

Human keratinocyte (HaCaT) cells were maintained in DMEM supplemented with 10% fetal bovine serum and incubated at 37 °C under a humidified atmosphere containing 5% CO_2. Cells were subcultured upon reaching appropriate confluency.

2.5.2 MTT Assay

Cytotoxicity of silver cholate metallogel formulations (SC-01 to SC-05) was assessed using the MTT assay. Cells previously grown in T-75 flasks were washed with PBS, trypsinized, and seeded into 96-well plates at a density of approximately 1000 cells per well in 200 µL of complete medium. Plates were incubated overnight to allow cell attachment.

After 24 h, the medium was replaced with serum-free DMEM containing varying concentrations of test samples (0.025%, 0.1%, 0.5%, and 1%). Solvent-treated cells served as negative controls, while appropriate positive controls were included in parallel. Following 24 h incubation, the medium was removed, cells were washed with PBS, and MTT solution (5 mg/mL in PBS) was added.

The plates were incubated for 2 h to allow formation of formazan crystals, which were subsequently dissolved in dimethyl sulfoxide (DMSO). Absorbance was measured at 570 nm using a microplate reader. Cell viability was calculated relative to solvent control, and experiments were performed in triplicate.

2.6 Antibacterial Activity Against *Cutibacterium acnes*

Antibacterial efficacy of silver cholate metallogel samples was evaluated using the **treat-and-plate method** against *Cutibacterium acnes*. Test samples were exposed to bacterial suspensions for a contact time of 3 minutes. Following exposure, serial dilutions were plated on appropriate agar media and incubated under anaerobic conditions.

Colony-forming units (CFU) were enumerated after incubation, and log reduction values were calculated relative to placebo controls. Percentage killing efficiency was derived from log reduction data to quantify antibacterial performance.

2.7 Minimum Inhibitory Concentration (MIC) Studies

2.7.1 MIC Against *Cutibacterium acnes*

MIC values against *C. acnes* were determined using the microdilution method. Serial dilutions of selected silver cholate metallogel formulations were prepared and incubated with standardized bacterial inocula. Clindamycin was used as a reference antibacterial agent. MIC was defined as the lowest concentration at which no visible bacterial growth was observed [47,48]

2.7.2 MIC Against *Malassezia furfur*

Antifungal activity was evaluated against *Malassezia furfur* using a similar microdilution protocol. Serially diluted samples were challenged with fungal suspensions, and growth inhibition was assessed after incubation. Fluconazole served as the reference for antifungal control. MIC values were reported as the minimum concentration required to inhibit visible fungal growth.

2.8 Statistical Analysis

All experiments were performed in triplicate unless otherwise specified. Data are reported as mean values. Qualitative and quantitative comparisons were made based on relative trends in cytotoxicity, antibacterial efficacy, and MIC values.

3. Results and Discussion

3.1 Visual Observation and Formation of Silver Cholate Metallogel

The formation of the silver cholate metallogel was initially evaluated through visual inspection and vial inversion tests. Upon dropwise addition of aqueous silver ion solution to sodium cholate solution, rapid transformation from a clear sol to a semi-opaque or opaque gel was observed, depending on the Ag^+ concentration. The gelation occurred under ambient conditions without the need for heating, pH adjustment, or external cross-linkers, highlighting the spontaneous nature of the coordination-driven self-assembly process [1,2,11].The concentration-dependent visual appearance and self-supporting nature of the metallogels (SC-01 to SC-05) are shown in **Figure 2.**

Photographic documentation of samples SC-01 to SC-05 clearly demonstrates concentration-dependent gel behavior. Lower silver concentrations resulted in weak or partially gelled systems, while higher Ag^+ content produced robust, self-supporting metallogels capable of maintaining their shape upon inversion. The progressive increase in opacity with increasing silver ion concentration suggests enhanced cross-linking density and network formation within the gel matrix.

This behavior can be attributed to coordination interactions between Ag^+ ions and the carboxylate groups of cholate, leading to the formation of extended three-dimensional networks. The absence of visible precipitation or phase separation indicates that silver ions are effectively immobilized within the supramolecular framework rather than forming bulk silver salts. Such controlled immobilization is particularly desirable for biomedical applications, where uncontrolled silver release can lead to cytotoxicity.

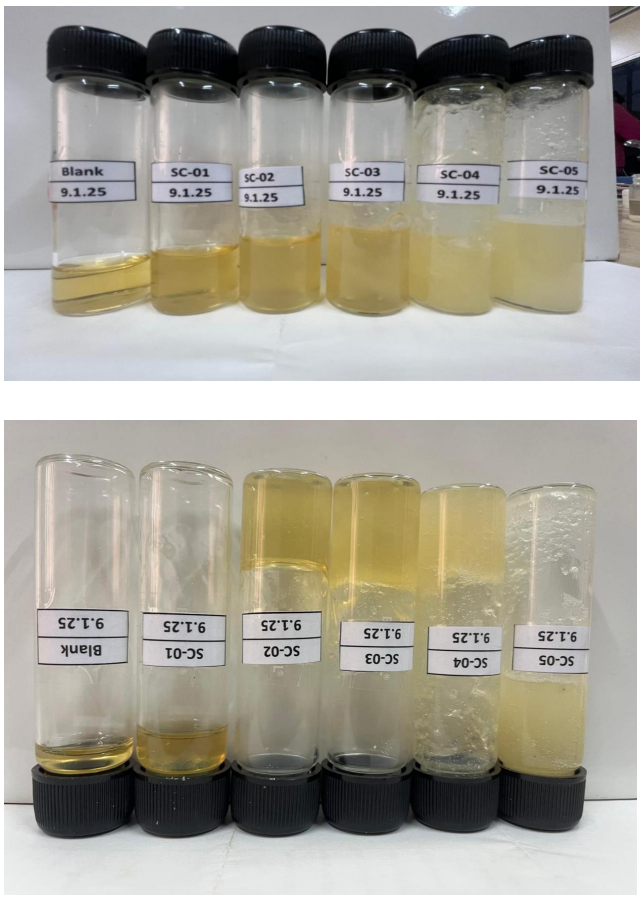

Figure 2. Visual appearance and gelation behavior of silver cholate metallogels prepared at different Ag^+ concentrations (SC-01 to SC-05), demonstrating concentration-dependent gel formation.

3.2 FTIR Spectroscopic Evidence of Silver–Cholate Coordination

FTIR spectra of $AgNO_3$, sodium cholate, and silver cholate metallogel are presented in **Figure 3.** FTIR spectroscopy was employed to elucidate the coordination mechanism underlying silver metallogel formation. Comparative spectra of silver nitrate, sodium cholate, and silver cholate metallogel provide clear evidence of successful metal–ligand interaction.

Sodium cholate exhibits characteristic asymmetric and symmetric stretching vibrations of the carboxylate group

at approximately 1578 cm^{-1} and 1404 cm^{-1}, respectively. These values are consistent with ionic COO^{-}–Na^{+} interactions typically observed in bile salts. Upon metallogel formation, these bands undergo noticeable shifts. In the silver cholate metallogel, the asymmetric COO^{-} stretching vibration shifts to higher wavenumbers (~1639 cm^{-1}), while the symmetric stretching band becomes broader and slightly shifted, resulting in a modified Δν value [36-38]

Such changes indicate coordination of Ag^{+} ions to the carboxylate moiety of cholate. The observed Δν values are consistent with predominantly monodentate or bridging coordination modes, which are commonly reported for silver carboxylate complexes. In addition, new absorption bands appear in the low-frequency region (400–500 cm^{-1}), which can be attributed to Ag–O stretching vibrations, further confirming silver incorporation into the cholate framework.

The broad O–H stretching band in the region of 3200–3600 cm^{-1} persists in the metallogel spectrum, albeit with slight broadening, suggesting that intermolecular hydrogen bonding among cholate hydroxyl groups remains intact. This combination of metal coordination and hydrogen bonding plays a crucial role in stabilizing the supramolecular gel network.

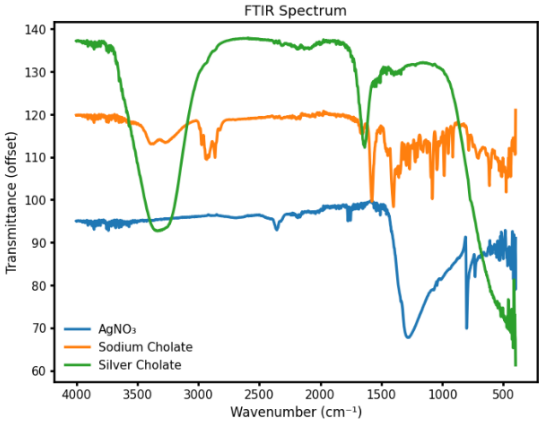

Figure 3. FTIR spectra of $AgNO_3$, sodium cholate, and silver cholate metallogel showing carboxylate coordination and Ag–O bond formation.

3.2.1 FTIR Spectroscopic Characterization of Silver Nitrate, Sodium Cholate, and Silver Cholate

Fourier-transform infrared (FTIR) spectroscopy was employed to elucidate the functional group characteristics and structural changes associated with the formation of silver cholate from silver nitrate ($AgNO_3$) and sodium cholate. Spectra were recorded in transmittance mode (%T) over the range of 4000–400 cm^{-1}, with data derived from experimental measurements provided for each compound. Peak assignments were based on observed absorption bands (corresponding to regions of low transmittance) and corroborated with literature values for similar systems. The analysis confirms the ion-exchange reaction, evidenced by the disappearance of nitrate vibrations, shifts in carboxylate modes indicative of silver coordination, and retention of the cholate organic scaffold.

3.2.2 FTIR Spectrum of Silver Nitrate ($AgNO_3$)

The FTIR spectrum of $AgNO_3$ exhibits characteristic vibrations primarily attributable to the nitrate anion (NO_3^{-}). A strong, broad absorption band centered at approximately 1281 cm^{-1} is assigned to the asymmetric stretching mode ($\nu_{as}(NO_3)$), consistent with reported values around 1278–1384 cm^{-1} for ionic nitrates. Additional bands at ~793 cm^{-1} and ~826 cm^{-1} correspond to the out-of-plane bending ($\delta(NO_3)$) and symmetric stretching ($\nu_s(NO_3)$) modes, respectively. Weaker features in the 400–500 cm^{-1} region, such as at ~463 cm^{-1}, may arise from Ag–O lattice vibrations or minor impurities. Notably, the spectrum lacks significant absorptions in the O–H (3400–3200 cm^{-1}) or C–H (3000–2800 cm^{-1}) regions, reflecting the inorganic nature of the compound. Minor artifacts, such as a peak at ~2357 cm^{-1}, are likely due to atmospheric CO_2 interference.

3.2.3 FTIR Spectrum of Sodium Cholate

Sodium cholate, a bile salt derived from cholic acid, displays a spectrum dominated by vibrations from its steroid backbone, hydroxyl groups, and carboxylate moiety. A broad absorption band at ~3381 cm^{-1} is attributed to O–H stretching (ν(OH)) from the multiple hydroxyl groups and potential hydration, with a full width at half-maximum indicative of hydrogen bonding. Aliphatic C–H stretching modes appear at ~2934 cm^{-1} (asymmetric $\nu(CH_3/CH_2)$) and ~2864 cm^{-1} (symmetric $\nu(CH_3/CH_2)$), consistent with the hydrophobic steroid ring system. The carboxylate group (COO^{-}) exhibits asymmetric and symmetric stretching bands at ~1578 cm^{-1} ($\nu_{as}(COO^{-})$) and ~1404 cm^{-1} ($\nu_s(COO^{-})$), respectively, with a frequency separation ($\Delta\nu \approx 174\ cm^{-1}$) suggesting ionic coordination to Na^{+}. Additional peaks include C–O stretches at ~1086 cm^{-1} and ~1042 cm^{-1} (from secondary alcohols), C–H bending at ~1294 cm^{-1} and ~1215 cm^{-1}, and skeletal vibrations in the fingerprint region (~984, ~949, and ~914 cm^{-1}). A minor band at ~1659 cm^{-1} may indicate adsorbed water ($\delta(H–O–H)$) or trace C=C modes. These features align with reported spectra for bile salts, confirming the presence of deprotonated carboxylic acid and amphiphilic structure.

3.2.4 FTIR Spectrum of Silver Cholate

The spectrum of silver cholate reveals modifications consistent with the substitution of Na^{+} by Ag^{+} in the cholate framework. The broad O–H stretch shifts slightly to ~3331 cm^{-1}, suggesting altered hydrogen bonding

environments possibly due to metal coordination or changes in hydration. C–H stretching bands remain largely preserved at ~2930–2860 cm^{-1}, indicating integrity of the steroid backbone. A prominent band at ~1639 cm^{-1} is assigned to the asymmetric carboxylate stretch ($\nu_{as}(COO^-)$), representing a shift from ~1578 cm^{-1} in sodium cholate, which may reflect bridging bidentate coordination (μ_2-OCO) to Ag^+. The symmetric carboxylate mode appears broadened around ~1400 cm^{-1}, with a reduced Δν supporting unidentate or bridging ligation typical of silver carboxylates. C–O stretches shift to lower wavenumbers (e.g., ~1040 cm^{-1} from 1046 cm^{-1}), implying weakening of these bonds due to Ag–O interactions. Enhanced absorptions in the metal-sensitive region (400–500 cm^{-1}), including bands at ~476, ~440, and ~430 cm^{-1}, are ascribed to Ag–O stretching vibrations, absent or weak in the precursors. These low-frequency modes confirm silver incorporation and stabilization by organic capping groups, analogous to fatty acid or protein-mediated stabilization in Ag nanocomplexes.

3.2.5 Comparative Analysis and Evidence of Reaction

Overlay of the spectra highlights key transformations indicative of successful ion exchange (Na-cholate + $AgNO_3$ → Ag-cholate + $NaNO_3$). The intense nitrate band at 1281 cm^{-1} in $AgNO_3$ is completely absent in silver cholate, confirming removal of NO_3^- and minimal residual precursor. Shifts in carboxylate frequencies (1578 → 1639 cm^{-1} for ν_{as}) and emergence of Ag–O modes underscore coordination of Ag^+ to the deprotonated carboxylate and possibly hydroxyl oxygens, promoting aggregation into nanocomplexes. The preservation of O–H and C–H regions between sodium cholate and silver cholate affirms no degradation of the bile salt structure, while subtle broadening suggests enhanced intermolecular interactions. These observations align with reports on bile salt-templated silver nanostructures, where hydrophobic-hydrophilic balance facilitates metal binding and stabilization.

In summary, FTIR analysis substantiates the synthesis of silver cholate as a coordination complex, with high purity inferred from the absence of extraneous peaks. This structural insight supports potential applications in nanotechnology, such as bile salt-capped silver nanoparticles for antimicrobial or imaging purposes. Further studies, including X-ray diffraction and electron microscopy, are recommended to corroborate these findings.

3.3 UV–Visible spectroscopic analysis

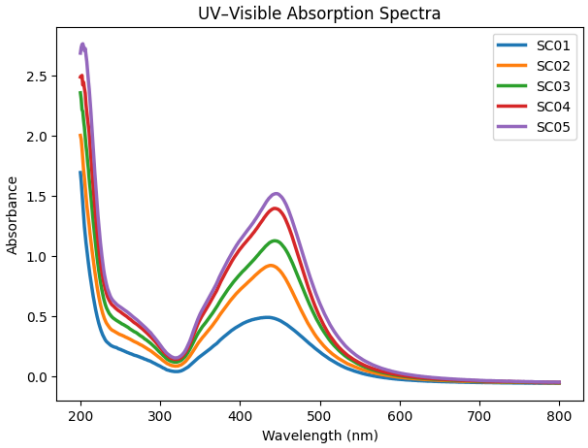

Figure 4. UV–Visible absorption spectra of silver cholate metallogel samples (SC01–SC05) recorded in the range of 200–800 nm, showing concentration-dependent absorbance and broad visible-region features associated with silver–cholate coordination.

The UV–Visible absorption spectra of silver cholate metallogel samples (SC-01 to SC-05) are shown in **Figure 4.**The UV–Visible absorption spectra of silver cholate samples (SC01, SC02, SC03, SC04, and SC05) were recorded in the range of **200–800 nm**. All samples exhibit a strong absorption band in the **UV region below 250 nm**, followed by a broader absorption feature extending into the **visible region (≈350–500 nm)**.

A systematic increase in absorbance intensity is observed with increasing silver content from SC01 to SC05, indicating concentration-dependent optical behavior. A broad absorption feature extending across the visible region (≈350–500 nm) was observed, with higher intensity and slight broadening for SC04 and SC05 compared to lower-concentration samples

Inference and Interpretation

UV region (<250 nm)

The intense absorption observed below 250 nm is attributed to **π–π*** and **n–π*** transitions associated with the cholate framework and ligand-to-metal charge transfer interactions involving coordinated Ag^+ ions.

Visible region (≈350–500 nm)

The appearance of a broad absorption band in the visible region suggests the formation of **silver–cholate coordination assemblies**. The absence of a sharp, narrow surface plasmon resonance (SPR) peak typical of metallic silver nanoparticles (~400–420 nm) indicates that **bulk Ag^0 nanoparticle formation is minimal or absent**.

Concentration-dependent behavior

The gradual increase in absorbance intensity from SC01 to SC05 reflects **enhanced silver incorporation within the cholate supramolecular network**, consistent with

coordination-driven metallogel formation rather than uncontrolled silver aggregation.

Correlation with FTIR and SEM results

The UV–Vis observations complement FTIR evidence of Ag–carboxylate coordination and SEM-revealed nanostructured morphology, collectively supporting the formation of a **silver-ion-stabilized supramolecular metallogel network**.

Biological relevance

The absence of a pronounced metallic SPR band is significant from a biological standpoint, as it suggests that silver is predominantly present in a **coordinated, immobilized form**, which aligns with the observed **reduced cytotoxicity** and **effective antimicrobial activity** in subsequent biological evaluations [18,20,14].

3.4 Morphological Analysis by Scanning Electron Microscopy

Scanning electron microscopy was used to examine the internal micro- and nanostructure of the silver cholate metallogel. SEM images reveal a densely packed, interconnected network composed of nanoscale particulate domains distributed uniformly across the surface.Representative SEM micrographs revealing the nanostructured morphology of the silver cholate metallogel are shown in **Figure 5.**

At higher magnifications, the metallogel exhibits a granular morphology with closely associated particles forming a continuous network. The absence of large crystalline aggregates suggests that silver ions are homogeneously distributed and effectively capped by cholate molecules, preventing uncontrolled crystallization. This morphology is consistent with coordination-driven self-assembly rather than phase-separated precipitation.

The observed nanostructured architecture provides a plausible explanation for the mechanical stability of the metallogel observed macroscopically. The interconnected particulate framework allows stress distribution throughout the network, enabling the gel to withstand deformation without collapse. Such nanostructured metallogels are particularly attractive for applications requiring both mechanical integrity and functional performance [4,39].

Mechanical integrity is inferred from the self-supporting behavior observed during vial inversion tests and the stable nanostructured morphology revealed by SEM; quantitative rheological evaluation will be addressed in future studies.

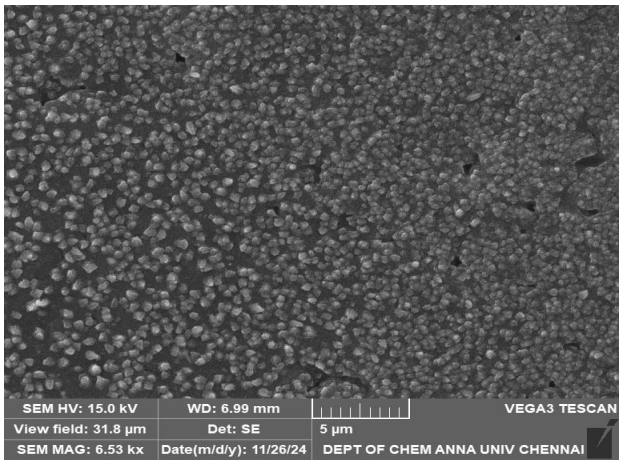

Figure 5. SEM micrograph of the silver cholate metallogel showing a densely packed nanostructured network responsible for mechanical stability.

SEM–EDX Elemental Analysis of SC-03:

Energy-dispersive X-ray (EDX) analysis of SC-03 confirmed the presence of silver and oxygen as the predominant elements within the analyzed region. The strong Ag signal verifies successful incorporation of silver within the cholate matrix, while the concurrent oxygen signal supports the presence of Ag–O interactions consistent with silver–carboxylate coordination observed in FTIR analysis. The absence of additional significant elemental peaks indicates chemical purity and suggests that silver is homogeneously distributed within the metallogel network.

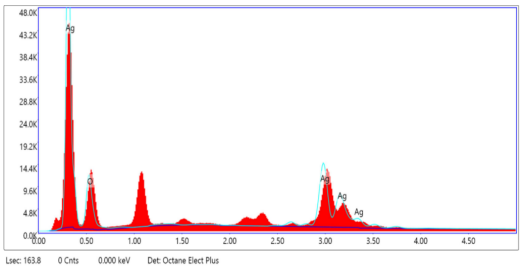

Figure 6. SEM–EDX spectrum of the silver cholate metallogel (SC-03) showing the presence of silver and oxygen. The prominent Ag Lα peak confirms silver-rich domains, while the O Kα signal indicates an oxygen-coordinated chemical environment, consistent with Ag–carboxylate interactions inferred from FTIR analysis.

3.5 Rheological Characterization of Silver Cholate Metallogels

The viscoelastic properties of silver cholate metallogels (SC-01 to SC-05) were evaluated by rotational and oscillatory rheology at 25 °C to quantitatively assess network formation and mechanical stability. Flow curve measurements conducted over a shear rate range of 0.1–100 s^{-1} revealed a progressive increase in apparent viscosity and the emergence of yield behavior with increasing silver content, indicating gradual

reinforcement of the supramolecular network across the series. The shear rate–dependent viscosity behavior of silver cholate metallogels (SC-01 to SC-05), illustrating shear-thinning characteristics and progressive viscosity enhancement with increasing silver content, is shown in **Figure 7.**

Oscillatory rheological measurements further highlighted the evolution from weakly structured systems to well-developed metallogels. Amplitude sweep experiments showed that SC-02 and SC-03 behave as soft physical gels, exhibiting moderate storage modulus (G′) values and relatively high deformability prior to yielding. In contrast, SC-04 and SC-05 displayed substantially higher G′ values, lower tan δ, and pronounced elastic dominance, confirming the formation of stronger and more rigid gel networks.The strain-dependent viscoelastic response of the metallogels, highlighting the linear viscoelastic region and yielding behavior, is presented in **Figure 8.** Notably, SC-04 yielded at lower strain compared to SC-05, suggesting a more brittle fracture behavior, whereas SC-05 demonstrated greater resistance to deformation.

Frequency sweep measurements provided additional insight into the viscoelastic nature of the metallogels. SC-01 exhibited pronounced frequency dependence of G′, characteristic of a weak physical gel or flocculated dispersion with limited long-range connectivity. In comparison, SC-04 and SC-05 showed nearly frequency-independent G′ plateaus over the measured angular frequency range, indicative of robust, percolated networks with dominant elastic response. Although complete frequency sweep data for SC-03 could not be acquired, the overall trend clearly establishes SC-05 as the strongest metallogel formulation in terms of rigidity and network stability. Frequency sweep measurements further elucidating the evolution from weakly structured systems to elastic, percolated gel networks are shown in **Figure 9.**

Collectively, these rheological findings provide quantitative support for the self-supporting behavior observed macroscopically and corroborate the nanostructured morphology revealed by SEM, establishing a clear structure–property relationship in the silver cholate metallogel system.

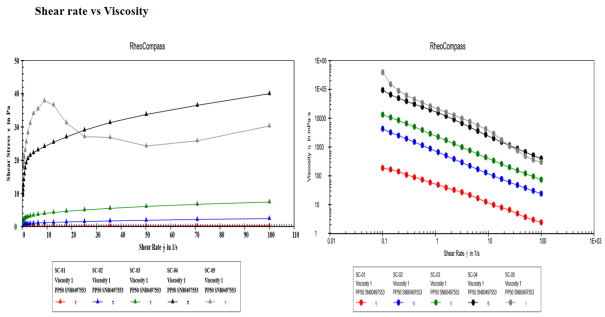

Figure 7. Flow curves of silver cholate metallogels (SC-01 to SC-05) measured at 25 °C over a shear rate range of 0.1–100 s^{-1}, showing progressive development of yield behavior and increased viscosity with increasing silver content.

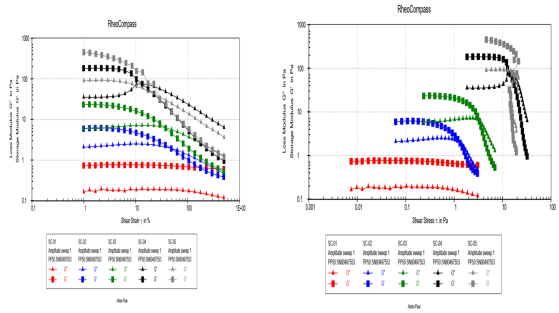

Figure 8. Oscillatory rheological characterization of silver cholate metallogels (SC-01 to SC-05) measured at 25 °C: Amplitude sweep conducted at a fixed angular frequency, showing strain-dependent yielding behavior and the evolution of elastic dominance with increasing silver content.

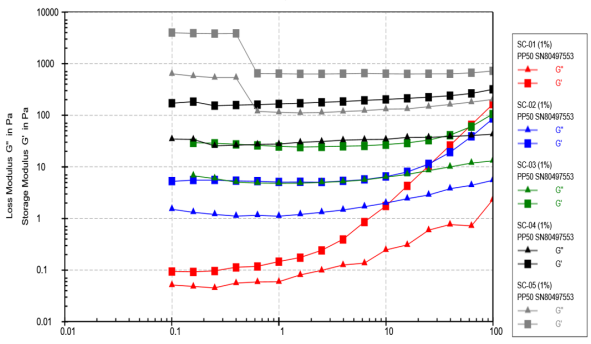

Figure 9. Oscillatory rheological characterization of silver cholate metallogels (SC-01 to SC-05) measured at 25 °C:Frequency sweep performed within the linear viscoelastic region, illustrating the transition from weakly structured systems to well-developed elastic gel networks with nearly frequency-independent storage modulus (G′) for higher-silver formulations.

3.6 Cytotoxicity Evaluation on HaCaT Human Keratinocyte Cells

Given the potential application of silver metallogels in skin-related formulations, cytotoxicity was evaluated using HaCaT human keratinocyte cells via the MTT assay. The results reveal a clear concentration-dependent cytotoxic response across different metallogel formulations [21-25]. The cytotoxicity profile of silver cholate metallogel formulations on HaCaT cells is summarized in **Table 2**.

Samples SC-01, SC-02, and SC-03 exhibited **no detectable cytotoxicity** across all tested concentrations (0.025–1%), indicating excellent biocompatibility. Importantly, SC-03 remained non-toxic even at 1% concentration, identifying it as the most biologically compatible formulation among the tested samples.

In contrast, SC-04 and SC-05 showed toxicity at higher concentrations, with SC-04 becoming toxic at 1% and SC-05 exhibiting toxicity at both 0.5% and 1%. This trend highlights the critical role of silver ion concentration in determining biological safety. While silver contributes antimicrobial activity, excessive silver availability can disrupt cellular metabolic processes, leading to reduced cell viability.

These results demonstrate that the silver cholate metallogel possesses a **well-defined safety window**, within which antimicrobial efficacy can be achieved without compromising keratinocyte viability. This balance between efficacy and safety is a key requirement for dermatological and topical applications.

Table 2. Cytotoxicity evaluation of silver cholate metallogel formulations on HaCaT human keratinocyte cells using the MTT assay.

Sample	Concentration (%)	Cell viability interpretation
SC-01	0.025	Non-toxic
	0.1	Non-toxic
	0.5	Non-toxic
	1.0	Non-toxic
SC-02	0.025	Non-toxic
	0.1	Non-toxic
	0.5	Non-toxic
	1.0	Non-toxic
SC-03	0.025	Non-toxic
	0.1	Non-toxic
	0.5	Non-toxic
	1.0	Non-toxic
SC-04	0.025	Non-toxic
	0.1	Non-toxic
	0.5	Non-toxic
	1.0	**Toxic**
SC-05	0.025	Non-toxic
	0.1	Non-toxic
	0.5	**Toxic**
	1.0	**Toxic**

3.7 Antibacterial Activity Against *Cutibacterium acnes*

The antibacterial efficacy of silver cholate metallogel formulations was evaluated against *Cutibacterium acnes* using the treat-and-plate method. All tested formulations demonstrated significant antibacterial activity within a short contact time of 3 minutes.

Quantitative analysis revealed log reductions ranging from approximately 2.08 to 3.71, corresponding to **99–99.9% bacterial killing efficiency**. Notably, SC-05 exhibited the highest log reduction (3.71), consistent with its higher silver content. However, SC-03 and SC-04 also achieved ~99% bacterial killing while maintaining superior cytocompatibility compared to SC-05. Quantitative antibacterial activity and log-reduction values against *C. acnes* are presented in **Table 3**.

The rapid antibacterial action observed suggests that silver ions embedded within the metallogel matrix remain accessible for interaction with bacterial cells. The cholate framework likely facilitates close contact between silver and bacterial membranes, enhancing antimicrobial efficiency while moderating silver release. These findings are particularly relevant for acne management, where rapid reduction of *C. acnes* populations is essential to control inflammation and lesion formation [26-30].

Table 3. Antibacterial activity of silver cholate metallogel formulations against *Cutibacterium acnes* determined by the treat-and-plate method.

Sample	Log value of sample	Log value of placebo	Log reduction	% Killing
Control-P	4.92	8.44	3.52	99.9
Control-N	4.98	8.44	3.46	99.9
SC-01	6.23	8.44	2.22	99
SC-02	6.20	8.44	2.24	99
SC-03	6.36	8.44	2.08	99
SC-04	6.34	8.44	2.10	99
SC-05	4.73	8.44	3.71	99.9

3.8 Minimum Inhibitory Concentration (MIC) Against *C. acnes*

MIC studies further confirmed the antibacterial potency of selected silver cholate metallogel formulations. SC-02 exhibited an MIC value of 312.5 µg/mL against *C. acnes*, while the thermally treated SC-05 formulation showed an MIC of 1250 µg/mL. Although clindamycin demonstrated a lower MIC, the silver metallogel offers the advantage of a non-antibiotic mechanism, reducing the risk of resistance development [27,30,47].

The MIC values corroborate the treat-and-plate results and support the potential of silver cholate metallogels as alternative or adjunct antimicrobial agents in acne treatment. Minimum inhibitory concentration (MIC) values for selected metallogel formulations against *C. acnes* are listed in **Table 4.**

Table 4. Minimum inhibitory concentration (MIC) of selected silver cholate metallogel formulations against *Cutibacterium acnes.*

Sample	MIC (µg/mL)
SC-02	312.5
SC-05 (70 °C treated)	1250
Clindamycin (control)	39.06

3.9 Antifungal Activity Against *Malassezia furfur*

The antifungal efficacy of silver cholate metallogels was assessed against *Malassezia furfur*, a fungus associated with dandruff and seborrheic dermatitis [31-35]. SC-03 exhibited a MIC value of 156.25 µg/mL, whereas SC-05 showed a higher MIC of 625 µg/mL. Although fluconazole remained more potent, the metallogel demonstrated meaningful antifungal activity.

The dual antibacterial and antifungal performance of the silver cholate metallogel highlights its potential for broad-spectrum skin applications, particularly in conditions involving mixed microbial flora. The antifungal MIC values against *Malassezia furfur* are summarized in **Table 5.**

Table 5. Minimum inhibitory concentration (MIC) of silver cholate metallogel formulations against *Malassezia furfur*.

Sample	MIC (µg/mL)
SC-01	1200
SC-02	625
SC-03	156.25
SC-04	156.25
SC-05	156.25
Fluconazole (control)	19.53

3.10 Structure–Property–Biological Correlation

The collective results establish a strong correlation between metallogel structure, silver coordination chemistry, and biological performance. FTIR and SEM analyses confirm the formation of a stable, nanostructured metallogel network that immobilizes silver ions while preserving controlled biological activity. Cytotoxicity and antimicrobial studies together identify SC-03 as an optimal formulation, combining high biocompatibility with effective antimicrobial action.

This structure–property–function relationship underscores the advantage of using bile salt–based metallogels as platforms for safe and effective silver delivery [39-43]. Unlike most reported silver-based soft materials that emphasize either physicochemical characterization or antimicrobial efficacy alone, the present work integrates coordination-driven gelation, concentration-resolved cytotoxicity profiling, and dual antibacterial–antifungal evaluation within a single bile salt–based metallogel system.

4. Conclusion

In this study, a **silver cholate–based metallogel** was successfully developed through a simple aqueous mixing strategy using commercially available sodium cholate and silver ions, without the need for multistep synthesis, polymeric supports, or external cross-linkers. The spontaneous gelation observed upon silver incorporation highlights the efficiency of coordination-driven self-assembly in bile salt systems.

Spectroscopic analysis using FTIR confirmed effective coordination between Ag^+ ions and the carboxylate groups of cholate, accompanied by preserved hydrogen-bonding interactions among hydroxyl groups. UV–Visible spectroscopic analysis further supported silver incorporation within the cholate supramolecular framework by showing broad visible-region absorption features and the absence of a sharp surface plasmon resonance band characteristic of bulk metallic silver. SEM imaging revealed a densely interconnected nanostructured network, providing a structural basis for the observed mechanical stability and self-supporting nature of the metallogel. Rheological characterization quantitatively confirmed the evolution from weakly structured systems to elastic metallogels with increasing silver content, supporting the observed macroscopic stability and supramolecular network formation.

Biological evaluation demonstrated a clear concentration-dependent safety profile. Selected formulations, particularly SC-03, exhibited excellent biocompatibility toward HaCaT human keratinocyte cells up to 1% concentration, while maintaining strong

antimicrobial efficacy. The silver metallogel showed rapid and significant antibacterial activity against *Cutibacterium acnes*, as well as antifungal activity against *Malassezia furfur*, confirmed through treat-and-plate assays and MIC determinations. Importantly, this antimicrobial performance was achieved without excessive cytotoxicity, indicating controlled silver availability within the supramolecular matrix.

Overall, the present work establishes a clear **structure–property–biological activity relationship** in silver cholate metallogels and demonstrates their potential as multifunctional soft materials for skin-related biomedical and topical applications [44-46,]. The simplicity of preparation, coupled with tunable biological performance, positions bile salt–based silver metallogels as promising alternatives to conventional silver delivery systems.

ACKNOWLEDGMENT

The authors are thankful to the Faculty of Pharmacy, Dr. M.G.R. Educational and Research Institute, Velappanchavadi, Chennai-600077, Tamil Nadu, India for providing the necessary lab facilities during the experimental study**.**

CONFLICT OF INTEREST

The author declares no conflict of interest.

DATA AVAILABILITY

Data will be made available on request.

LIMITATIONS

Limited data availability

ETHICAL APPROVAL

This study does not involve any animal or human subjects.

REFERENCES:

1. Tam, A. Y. Y.; Yam, V. W. W. Recent advances in metallogels. Chem. Soc. Rev. 2013, 42, 1540–1567. https://doi.org/10.1039/C2CS35354G
2. Du, X.; Zhou, J.; Shi, J.; Xu, B. Supramolecular Hydrogelators and Hydrogels: From Soft Matter to Molecular Biomaterials. Chem. Rev. 2015, 115, 13165–13307. https://doi.org/10.1021/acs.chemrev.5b00299
3. Draper, E. R.; Adams, D. J. Low-molecular-weight gels: the state of the art. Chem 2017, 3, 390–410. https://doi.org/10.1016/j.chempr.2017.07.012
4. Terech, P.; Weiss, R. G. Low Molecular Mass Gelators of Organic Liquids and the Properties of Their Gels. Chem. Rev. 1997, 97, 3133–3160. https://doi.org/10.1021/cr9700282
5. Steed, J. W. Supramolecular gel chemistry: developments over the last decade. Chem. Commun. 2011, 47, 1379–1390. https://doi.org/10.1039/C0CC03293J
6. Draper, E. R.; Adams, D. J. How should multicomponent supramolecular gels be characterised? Chem. Soc. Rev. 2018, 47, 3395–3405. https://doi.org/10.1039/C7CS00804J
7. Kumar, D. K.; Steed, J. W. Supramolecular gel phase crystallization: orthogonal self-assembly under non-equilibrium conditions. Chem. Soc. Rev. 2014, 43, 2080–2088. https://doi.org/10.1039/C3CS60224A
8. Buerkle, L. E.; Rowan, S. J. Supramolecular gels formed from multi-component low molecular weight species. Chem. Soc. Rev. 2012, 41, 6089–6102. https://doi.org/10.1039/C2CS35106D
9. Raeburn, J.; Adams, D. J. Multicomponent low molecular weight gelators. Chem. Commun. 2015, 51, 5170–5180. https://doi.org/10.1039/C4CC08626K
10. Contreras-Montoya, R.; et al. Supramolecular gels: a versatile crystallization toolbox. Chem. Soc. Rev. 2024, 53, 7645–7673. https://doi.org/10.1039/D4CS00271G
11. Goldshleger, N. F.; et al. Supramolecular gels based on bile acid salts. Russ. Chem. Rev. 2017, 86, 1137–1162. https://doi.org/10.1070/RCR4682
12. Madenci, D.; Egelhaaf, S. U. Self-assembly in aqueous bile salt solutions. Curr. Opin. Colloid Interface Sci. 2010, 15, 109–115. https://doi.org/10.1016/j.cocis.2009.11.010
13. Zhang, M.; et al. Supramolecular hydrogelation with bile acid derivatives: structures, properties and applications. J. Mater. Chem. B 2016, 4, 7506–7520. https://doi.org/10.1039/C6TB02270G
14. Bariya, D.; et al. Recent advances in the bile acid based conjugates/derivatives towards their gelation applications. Steroids 2021, 166, 108769. https://doi.org/10.1016/j.steroids.2020.108769
15. Deacon, G. B.; Phillips, R. J. Relationships between the carbon–oxygen stretching frequencies of carboxylato complexes and the type of carboxylate coordination. Coord. Chem. Rev. 1980, 33, 227–250. https://doi.org/10.1016/S0010-8545(00)80455-5
16. Nara, M.; et al. Infrared spectroscopic study of metal coordination of the carboxylate group. Biochem. Biophys. Res. Commun. 2008, 369, 225–239. https://doi.org/10.1016/j.bbrc.2007.11.188
17. Wulandari, P.; et al. Coordination of Carboxylate on Metal Nanoparticles Characterized by FTIR Spectroscopy. Chem. Lett. 2008, 37, 888–889. https://doi.org/10.1246/cl.2008.888

18. Morones, J. R.; et al. The bactericidal effect of silver nanoparticles. Nanotechnology 2005, 16, 2346–2353. https://doi.org/10.1088/0957-4484/16/10/059
19. Rai, M.; et al. Silver nanoparticles as a new generation of antimicrobials. Biotechnol. Adv. 2009, 27, 76–83. https://doi.org/10.1016/j.biotechadv.2008.09.002
20. Tang, S.; Zheng, J. Antibacterial Activity of Silver Nanoparticles: Structural Effects. Adv. Healthc. Mater. 2018, 7, 1701503. https://doi.org/10.1002/adhm.201701503
21. Le Ouay, B.; Stellacci, F. Antibacterial activity of silver nanoparticles: A surface science insight. Nano Today 2015, 10, 339–354. https://doi.org/10.1016/j.nantod.2015.04.002
22. Franci, G.; et al. Silver Nanoparticles as Potential Antibacterial Agents. Molecules 2015, 20, 8856–8874. https://doi.org/10.3390/molecules20058856
23. Bruna, T.; et al. Silver Nanoparticles and Their Antibacterial Applications. Int. J. Mol. Sci. 2021, 22, 7202. https://doi.org/10.3390/ijms22137202
24. Marambio-Jones, C.; Hoek, E. M. V. A review of the antibacterial effects of silver nanomaterials. J. Nanopart. Res. 2010, 12, 1531–1551. https://doi.org/10.1007/s11051-010-9900-y
25. Lansdown, A. B. G. Silver in health care: antimicrobial effects and safety in use. Curr. Probl. Dermatol. 2006, 33, 17–34. https://doi.org/10.1159/000093928
26. Drake, P. L.; Hazelwood, K. J. Exposure-related health effects of silver and silver compounds. Ann. Occup. Hyg. 2005, 49, 575–585. https://doi.org/10.1093/annhyg/meh100
27. Hadrup, N.; Lam, H. R. Oral toxicity of silver ions, silver nanoparticles and colloidal silver. Regul. Toxicol. Pharmacol. 2014, 68, 1–7. https://doi.org/10.1016/j.yrtph.2013.11.002
28. Reidy, B.; et al. Mechanisms of silver nanoparticle release, transformation and toxicity. J. R. Soc. Interface 2013, 10, 20130442. https://doi.org/10.1098/rsif.2013.0442
29. Fox, C. L. Silver sulfadiazine—a new topical therapy for pseudomonas in burns. Arch. Surg. 1968, 96, 184–188. https://doi.org/10.1001/archsurg.1968.01330280020004
30. Prasher, P.; et al. Silver nanoparticles as antimicrobial therapeutics. 3 Biotech 2018, 8, 411. https://doi.org/10.1007/s13205-018-1436-3
31. Ochsendorf, F. Cutibacterium acnes in acne pathophysiology. Br. J. Dermatol. 2019, 180, 1003–1004. https://doi.org/10.1111/bjd.18316
32. Platsidaki, E.; Dessinioti, C. Recent advances in understanding Cutibacterium acnes. F1000Research 2018, 7, 1953. https://doi.org/10.12688/f1000research.15659.1
33. Byrd, A. L.; et al. The human skin microbiome. Nat. Rev. Microbiol. 2018, 16, 143–155. https://doi.org/10.1038/nrmicro.2017.157
34. Dréno, B.; et al. The role of Cutibacterium acnes in acne vulgaris. J. Eur. Acad. Dermatol. Venereol. 2018, 32, 5–15. https://doi.org/10.1111/jdv.15043
35. Guo, Y.; et al. Photodynamic therapy treats acne by altering the skin microbiota. Skin Res. Technol. 2023, 29, e13269. https://doi.org/10.1111/srt.13269
36. Gaitanis, G.; et al. The Malassezia genus in skin and systemic diseases. Clin. Microbiol. Rev. 2012, 25, 106–141. https://doi.org/10.1128/CMR.00021-11
37. Saunte, D. M. L.; et al. Malassezia-associated skin diseases. Front. Cell. Infect. Microbiol. 2020, 10, 112. https://doi.org/10.3389/fcimb.2020.00112
38. Harada, K.; et al. Malassezia species and their associated skin diseases. J. Dermatol. 2015, 42, 522–531. https://doi.org/10.1111/1346-8138.12700
39. Wikramanayake, T. C.; et al. Seborrheic dermatitis—looking beyond Malassezia. Exp. Dermatol. 2019, 28, 991–1001. https://doi.org/10.1111/exd.14006
40. Winter, H. H.; Chambon, F. Analysis of linear viscoelasticity of a crosslinking polymer at the gel point. J. Rheol. 1986, 30, 367–382. https://doi.org/10.1122/1.549853
41. Mosmann, T. Rapid colorimetric assay for cellular growth and survival. J. Immunol. Methods 1983, 65, 55–63. https://doi.org/10.1016/0022-1759(83)90303-4
42. Boukamp, P.; et al. Normal keratinization in a spontaneously immortalized aneuploid human keratinocyte cell line (HaCaT). J. Cell Biol. 1988, 106, 761–771. https://doi.org/10.1083/jcb.106.3.761
43. Wiegand, I.; et al. Agar and broth dilution methods to determine the minimal inhibitory concentration (MIC). Nat. Protoc. 2008, 3, 163–175. https://doi.org/10.1038/nprot.2007.521
44. Andrews, J. M. Determination of minimum inhibitory concentrations. J. Antimicrob. Chemother. 2001, 48 (Suppl. 1), 5–16. https://doi.org/10.1093/jac/48.suppl_1.5
45. Goor, O. J. G. M.; et al. From supramolecular polymers to multi-component biomaterials. Chem.

Soc. Rev. 2017, 46, 6621–6637. https://doi.org/10.1039/C7CS00564D

46. Chakrabarty, A.; et al. Metal cholate hydrogels: versatile supramolecular systems for nanoparticle embedded soft hybrid materials. J. Mater. Chem. 2012, 22, 18285–18294. https://doi.org/10.1039/C2JM34016J
47. Laishram, R.; et al. A Stimuli-Responsive Metallohydrogel Exhibiting Cyclohexane-Like Hydrophobicity. Chem. Asian J. 2017, 12, 1811–1818. https://doi.org/10.1002/asia.201700289
48. Kumar, A.; et al. Design, preparation and applications of gel nanocomposites from bile acids – A brief review. J. Indian Chem. Soc. 2021, 98, 100222. https://doi.org/10.1016/j.jics.2021.100222
49. Kumar, A.; Maitra, U. Recent advances in bile acid-derived supramolecular gels and their applications. J. Indian Chem. Soc. 2020, 97, 123–132.https://doi.org/10.1016/j.jics.2021.100222